Journal of Colloid and Interface Science 486 (2017) 219–231

Contents lists available at ScienceDirect

Journal of Colloid and Interface Science

journal homepage: www.elsevier.com/locate/jcis

Electro-osmosis in inhomogeneously charged microporous media by pore-scale modeling

Li Zhang, Moran Wang *

Department of Engineering Mechanics and CNMM, Tsinghua University, Beijing 100084, China

GRAPHICAL ABSTRACT

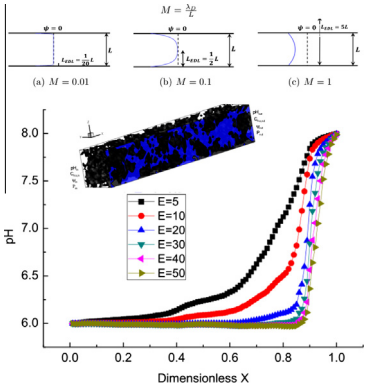

ARTICLE INFO

Article history:
Received 23 July 2016
Revised 6 September 2016
Accepted 25 September 2016
Available online 29 September 2016

Keywords:
Electro-osmosis
Inhomogeneous charge
Pore-scale modeling
Microporous media
Thin electrical double layer model

ABSTRACT

Surface charge at solid-electrolyte interface is generally coupled with the local electrolyte properties (ionic concentration, pH, etc.), and therefore not as assumed homogeneous on the solid surfaces in the previous studies. The inhomogeneous charge brings huge challenges in predictions of electro-osmotic transport and has never been well studied. In this work, we first propose a classification of electro-osmosis based on a dimensionless number which is the ratio of the Debye length to the characteristic pore size. In the limit of thin electrical double layer, we establish a pore-scale numerical model for inhomogeneously charged electro-osmosis including four ions: Na^+, Cl^-, H^+ and OH^-. Based on reconstructed porous media, we simulate the electro-osmosis with inhomogeneous charge using lattice Boltzmann method. The nonlinear response of electro-osmotic velocity to applied electrical field and the reverse flow have been observed and analyzed.

1. Introduction

Electro-osmosis in porous media has been studied for over 200 years due to its important applications in soil, petroleum and chemical engineering [1,2] since it was first observed in 1809 by Reuss [3]. For examples, as a non-mechanical pumping technique, electro-osmosis is widely used in sludge dewatering (e.g., [4]), capillary chromatography (e.g., [5,6]), membrane filtration (e.g., [7]), electrokinetic remediation (e.g., [8,9]) and microfluidic devices (e.g, [10,11]). Recent developments in nanotechnology also raise interest to explore more possibilities in making use of electro-osmosis and other related electrokinetic phenomena for energy conversion (e.g., [12,13]), desalination (e.g., [14]) or

* Corresponding author.
E-mail address: mrwang@tsinghua.edu.cn (M. Wang).

http://dx.doi.org/10.1016/j.jcis.2016.09.057
0021-9797/

biological use (e.g., [15]). Besides, from the thermodynamic point view, the electro-osmotic permeability is closely related to the electrical conductivity, hydraulic permeability and streaming current coupling coefficient, which are important properties in geophysical exploration (e.g., [16–19]).

Up to date, the most commonly used relation for electro-osmosis in porous media is the Helmholtz-Smoluchowski (HS) equation, which is introduced by Smoluchowski in 1905 [20]. Generally, the applicability of HS equation is constrained by three main assumptions. Firstly, the characteristic length of the electrical double layer (EDL) is much smaller than the pore size, namely, the thin double layer assumption. Secondly, the surface conductance, or the double layer conductance has little contribution to the total ionic conductance. Since the surface conductance increases with absolute value of zeta potential $|\zeta|$ and bulk concentration, this poses an upper limit on $|\zeta|$ [21] and bulk concentration. Thirdly, the solid/liquid interface is homogeneously charged, which is often implicitly employed by introducing a constant surface potential or surface charge density. Although numerous work has been done to lift the limitation of the original HS equation, just to name a few of them, Overbeek and Wijga [22], Burgreen and Nakache [23], Rice and Whitehead [24], Levine et al. [25], O'Brien [21], a general framework is still lacking and challenging, especially when the thin double layer assumption fails.

The thickness of electrical double layer relative to the pore size plays a key role in determining the property of electro-osmosis. Most of the useful results are derived for thin double layer limit, such as the HS equation. Other than this, when the thickness of EDL is comparable, or even larger than the pore size, namely, in the thick double layer limit, the diffuse layer potential distribution can be seen as uniform across the pore space. By averaging over the cross-section (for nanochannel) (e.g., [26]) or volume averaging (for porous media) (e.g., [27]), the 3D problem reduces to 1D. This thick double layer model is often referred as Donnan model owing to the fact that Donnan equilibrium is assumed at the inlet and outlet. Although the validity of these approximated models (thin double layer model and thick double layer model) have been justified by various theoretical and experimental study (e.g. [28]), there has not been any general criteria to systematically clarify the scope of these approximations. In an analogy to classification for fluid mechanics based on the Knudsen number, we propose a general classification for electro-osmosis for the first time based on the ratio of Debye length to characteristic physical size, which can be used as a guideline for simplifying physical model for electro-osmosis.

In most previous work, it is common to assume, in priori, homogeneous charge, i.e., constant surface charge density or surface potential, on the solid-liquid interface (e.g., [29,30]). Nevertheless, since the charging process is closely related to chemical equilibrium between surface and local bulk solution, the amount of surface charge is dependent on the property of local bulk solution, such as concentration and pH. Consequently, the homogeneous charge assumption may fail if the property of electrolyte solution is not homogeneous in the pore space. This will lead to the case of inhomogeneously charged electro-osmosis.

In terms of micro- and nanofluidics, inhomogeneously charged electro-osmosis has been studied for purpose of active control of flow pattern (e.g., [31–33]). In membrane science, previous results show that the inhomogeneity in charge density can have significant influence on current efficiency (e.g., [34]). What's more, study on electrokinetic remediation and soil consolidation in civil engineering have recognized the effect of inhomogeneous charge because of the gradient of pH for a long time (e.g., [35,36]). Some macroscopic models have been proposed by including the geochemical reactions (e.g., [37,38]). Lemaire et al. [39] and de Lima et al. [40–42] coupled surface protonation/deprotonation reactions to microscopic transport model and employed homogenization method to provide the effective parameters for macroscopic model. However, they only solve the closure problem for 2D straight channel. Recent work by Zhang and Wang [43] modify the space charge model to include the effects of heterogeneous charge along the nanochannel to study reverse electrodialysis. In summary, to the authors' knowledge, the effects of inhomogeneous charge on electro-osmotic flow in complex porous structures have not been well studied.

The challenges of inhomogeneously charged electro-osmosis lie in the coupling of surface charge boundary and local transport property and complex geometry of porous media. Based on the classification for electro-osmosis, we attempt to simplify the model and provide a strategy to determine local transport property for inhomogeneously charged electro-osmosis in porous media, which will be described in detail in Section 2.

In terms of structure of porous media, simplified models of porous structures, such as capillary tube model (e.g., [22,44]) and cell model (e.g., [45–47]) have been used to obtain analytical or semi-analytical solution for electro-osmotic permeability. Although recent development of imaging techniques such as micro-CT scanning, provides us the opportunity to recover the realistic micro structure of porous media [48], its use is still limited by high cost. As a cheaper and more flexible alternative, numerical reconstruction methods reproduce microporous structures by computer algorithms [49–51]. Meanwhile, owing to the advent of super computers, numerical simulation can handle with more complex structures of porous media and provide a powerful tool to study pore-scale transport process in porous media such as electro-osmosis (e.g. [29,52,30,53]). In these models, the detailed information in the pore space can be accurately captured and the transport property can be evaluated by averaging over the sample. In this work, we first reproduce random porous structures by random generation growth method (RGG) [54] and solve for the pore-scale distribution using lattice Boltzmann method [55].

This paper is organized as follows. Section 2 describes the classification criteria for electro-osmosis. Sections 3 and 4 present the theoretical preparation and numerical model for inhomogeneously charged electro-osmosis. Results and discussion are given in Section 5. Section 6 concludes this work.

2. Classification of electro-osmosis

The challenge of inhomogeneously charged electro-osmosis comes from the coupling of surface charge boundary and the "local" fluid properties in transport, and the difficulties lie in the following key questions. (i) Are the electrical double layers overlapped in the pores? The answer of this question determines the availability of local electroneutrality and validity of the bulk properties to calculate the surface charge. (ii) Does the charge structure within the electrical double layer play an important role to the transport? If the answer is no, the solution may be significantly simplified, for both non-overlapped or fully overlapped cases. (iii) Is the conventional simple model still valid? Once there is any possibility for the conventional models still available, efforts for extension by modifications may be highly appreciated and recognized by engineering applications. Since a general solution has so many difficulties and has never been established for all cases effectively, a classification of electro-osmosis in inhomogeneously charged porous media is necessary to clarify the solubility.

Based on the analysis to the challenges, the answers to the questions seem all dependent of the thickness of electrical double layer (L_{EDL}) locally compared with the characteristic pore size (L), as shown in Fig. 1(a), where λ_D is the Debye length. To characterize the thickness of EDL quantitatively, we define a non-dimensional

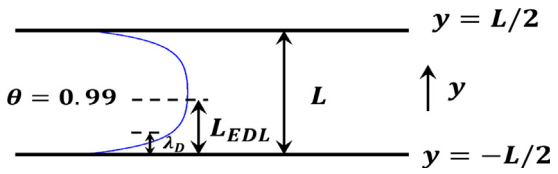

(a) Lengths in physical model. L is the characteristic length of pore. L_{EDL} is the thickness of electrical double layer and λ_D is the Debye length. The blue line is the electrical potential profile and θ is the non-dimensional excess electrical potential.

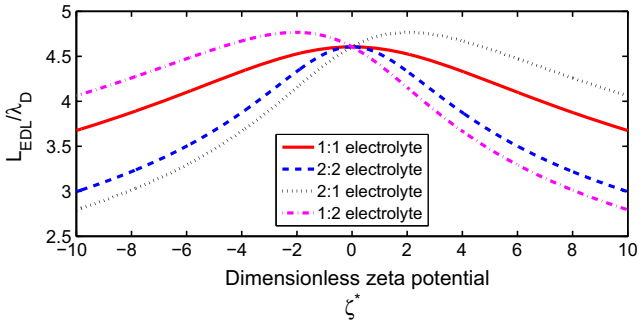

(b) Ratio between EDL length and Debye length L_{EDL}/λ_D against dimensionless zeta potentials ζ^* for different types of electrolyte. The ratio is lower than but close to 5 for all cases.

Fig. 1. Illustration of definition of different lengths (a) and ratio between EDL length and Debye length (b).

excess electrical potential, $\theta = \frac{\psi - \zeta}{\zeta}$, where ψ is the electrical potential and ζ is the zeta potential. Similar to the definition of boundary layer thickness in fluid mechanics, the thickness of electrical double layer is defined as the position where the excess electrical potential is 0.99, i.e., $\theta = 0.99$. Thus the thickness of EDL can be determined quantitatively. Fig. 1(b) shows that the ratio of thickness of EDL relative to Debye length, L_{EDL}/λ_D, is not a constant but varies with zeta potential and type of solutions. In all cases, the ratio is below but close to 5. Therefore, one can roughly estimate L_{EDL} as five times of λ_D.

It is easy to associate this ratio of two size with another well-known one, the Knudsen number Kn which is defined as ratio of gas molecular mean free path to the characteristic geometric length in gas transport. The Knudsen number helps to classify gas flow into four regimes[56,57]: (i) the continuum regime at $Kn \leqslant 0.01$ where the classical theories of fluid mechanics are available; (ii) the slip regime at $0.01 < Kn \leqslant 0.1$ where the continuum theories begin to break down but the modifications with slip boundary conditions may work; (iii) the transition regime at $0.1 < Kn \leqslant 10$ where the continuum assumption totally breaks down and the transport behavior has to be captured by molecule-based and statistical methods; and (iv) the free-molecular regime at $Kn > 10$ where the gas molecular collision is rare at movement so that some simple analytical solution can be established again.

Inspired by Kn, we propose here a dimensionless number, $M = \frac{\lambda_D}{L}$, to distinguish different regimes of electro-osmosis, where λ_D is the Debye length and L is the characteristic geometric length (e.g., local or mean pore size). Here we use the Debye length instead of the thickness of electrical double layer (L_{EDL}) because the Debye length can be directly determined by the theoretical formula (e.g., [2]). Based on M, the electro-osmotic flow can be divided into four regimes as well:

- thin layer regime ($M \leqslant 0.01$),
- non-overlap layer regime ($0.01 < M \leqslant 0.1$),
- partially-overlap layer regime ($0.1 < M \leqslant 1$),
- fully-overlap layer regime ($M > 1$).

The profiles of electrical potential for three typical values of M are shown in Fig. 2.

In the thin layer regime at $M \leqslant 0.01$, the thickness of EDL is much smaller than the characteristic geometric length so that the charge structure within EDL is negligible. Most pore region remains electroneutral and bulk properties. The velocity profile appears plug-like. In this regime, the classical Helmholtz-Smoluchowski (HS) equation [58] is available to introduce a slip velocity on wall surfaces dependent on the local charge and solution properties by:

$$\boldsymbol{u}_{HS} = -\frac{\epsilon\zeta}{\mu}\boldsymbol{E}, \tag{1}$$

where μ is the dynamic viscosity and ϵ is the permittivity of electrolyte solution, ζ is the local zeta potential of surface, and $\boldsymbol{E}$ is the local electrical strength.

In the non-overlap regime at $0.01 < M \leqslant 0.1$, the thickness of EDL is still smaller than the characteristic geometric length. However the charge distribution structure within EDL is not negligible and has to be fully solved. The consequent velocity profile may change from plug-like to parabolic-like. Since still no overlap of EDLs in this regime, the local bulk property of fluid can be taken at the middle of the pore. In this regime, the conventional simple models, such the HS model for slip velocity on surfaces, are not valid rigorously; however as M is not so large, modifications to the macroscopic models are still available for rough estimation at an acceptable accuracy. This strategy is similar to the slip modification to the continuum model for gas flow at $0.01 < Kn < 0.1$. Here we introduce a dimensionless correction factor Θ to modify the thin double layer model. Θ is defined as the ratio of cross-section averaged velocity, u_{avg}, to the Helmholtz-Smoluchowski velocity, u_{HS}, i.e. $\Theta = \frac{u_{avg}}{u_{HS}}$. In this non-overlap regime, the electrical potential in the middle remains zero so that the analytical solution for velocity field can be obtained. With some approximations for the integral, we propose a relationship of Θ at the analytical form for a 1:1 type electrolyte by

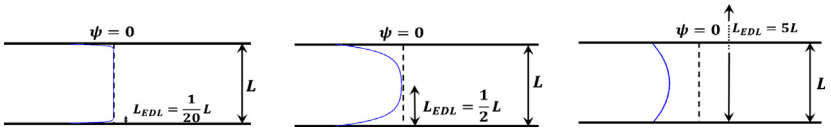

(a) $M = 0.01$ (b) $M = 0.1$ (c) $M = 1$

Fig. 2. Classification of electro-osmosis based on $M = \frac{\lambda_D}{L}$. Blue lines represent profiles of electrical potential. (For interpretation of the references to color in this figure legend, the reader is referred to the web version of this article.)

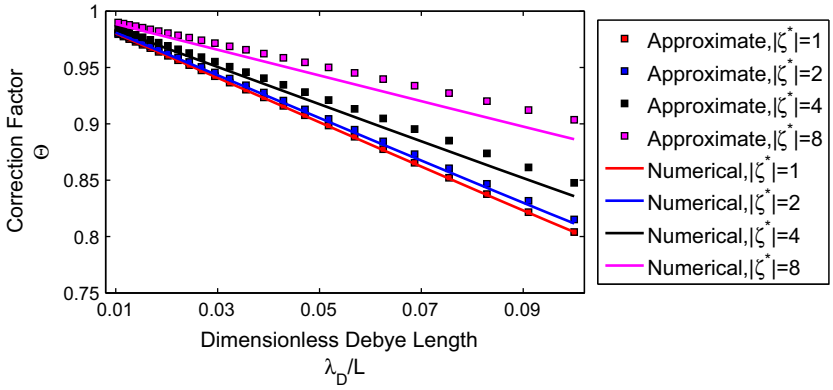

Fig. 3. Correction factor for dimensionless Debye length $\in [0.01, 0.1]$ with different dimensionless zeta potentials. Symbols denote the approximate results using Eq. (2), while lines denote accurate results by numerical modeling.

$$\Theta = 1 - \frac{8M}{\zeta^*}\tanh\left(\frac{\zeta^*}{4}\right), \tag{2}$$

where ζ^* is the dimensionless zeta potential normalized by $\frac{k_B T}{e}$. For $|\zeta^*| < 1, \Theta$ can be further simplified to $1 - 2M$. For $|\zeta^*| > 8, \Theta$ can be approximated by $1 - \frac{10M}{\zeta^*}$. Detailed derivation can be found in Appendix A. Fig. 3 shows the predicted averaged velocity across a 2D straight channel by the modified HS model, Eq. (2), compared with the accurate results by numerical modeling. It is not surprising to find the deviations increase with the dimensionless Debye length and zeta potential, but the acceptable agreement at a large range of ζ^* and λ_D/L proves the good performance of our correction factor formula.

In the partially-overlapped regime at $0.1 < M < 1$, the interaction between EDLs occurs and there is no electroneutral region in the whole pore. The charge structure and flow velocity have to be fully solved by numerical methods and no simple analytical solution is available for this situation.

In the fully-overlap regime at $M > 1$, the thickness of EDL is much larger than the geometric length and the EDLs are fully overlapped. In this case, since the electrical potential in the pore space is similar to zeta potential, the whole region can be treated as equipotential. The local bulk property in this case has to be determined by external conditions. Again some simple models can be established for predictions. For example, in the pore-network model [53], the property in the throat/channel can be determined by the connected pores or reservoirs.

Compared with the few previous studies, as shown by Jackson and Leinov [28], for study of streaming potential using capillary model, the thin double layer model is valid for $M < 0.0025$ ($M < 0.01$ in this work) and the thick double layer assumption is valid for $M > 3$ ($M > 1$ in this work). This good agreement reflects the intimate relation between electro-osmosis and streaming potential.

The classification based on M makes the very complicated problem into several solvable pieces. In this study as the first step, we focus on the thin layer regime at $M \leqslant 0.01$. We will build up a theoretical and numerical framework to predict electro-osmotic flow behavior in inhomogeneously charged porous media when the classical HS model is still valid. Actually the significance of classification based on M is far beyond just providing a strategy to investigate inhomogeneously charged electro-osmosis. On the one hand, previous models and results can be categorized according to the value of M, which will be convenient for use. On the other hand, for a new problem, M can be first estimated to obtain a simplified problem. In this way, M serves as a guideline for future research.

3. Mathematical models

3.1. Fluid flow

For electro-osmotic flow of aqueous electrolyte solution in microporous media, the flow is generally laminar and incompressible (e.g., [2,30]). The governing equations for fluid flow are,

$$\nabla \cdot \boldsymbol{u} = 0, \tag{3}$$

$$\frac{\partial \boldsymbol{u}}{\partial t} + \boldsymbol{u} \cdot \nabla \boldsymbol{u} = -\frac{\nabla p}{\rho} + \nu \nabla^2 \boldsymbol{u} + \frac{\boldsymbol{F}_E}{\rho}, \tag{4}$$

where $\boldsymbol{u}$ is the fluid velocity in pores, ν the kinematic viscosity, p the pressure, ρ the density and $\boldsymbol{F}_E$ a body force induced by the external electrical field. For the slipping model with $M \leqslant 0.01$ concerned in this work, the electrical body force reduced to the slip velocity on the surface, which is determined by the HS equation as shown in Eq. (1).

3.2. Surface charge distribution

Rather than employing a given zeta potential at liquid–solid interfaces, such as in Wang and Chen [30], we determine zeta potential at the interface by introducing surface complexation model. Following de Lima et al. [40–42], we use a 1-pK model instead of more complicated models, such as the triple layer model (e.g., [27,19]), for simplicity as the first step in this work, which considers a single protonation/deprotonation chemical reaction,

$$(>\mathrm{Me-OH})^{-1/2} + \mathrm{H}^+ \leftrightarrow (>\mathrm{Me-OH_2})^{+1/2}, \tag{5}$$

where Me represents a metallic ion lying in the tetrahedral (Si^{+4}) or octahedral (Al^{+3}) layers of clay particle.

Dynamic equilibrium of surface complexation reaction leads to the correlation between surface charge density σ and zeta potential ζ [42],

$$\sigma = \frac{F\Gamma_{MAX}}{2}\left(\frac{KC^b_{\mathrm{H}+}\exp\left(-\frac{F\zeta}{RT}\right) - 1}{KC^b_{\mathrm{H}+}\exp\left(-\frac{F\zeta}{RT}\right) + 1}\right), \tag{6}$$

where

$$K := \frac{\gamma_{\{(>\mathrm{Me-OH_2})^{+1/2}\}}}{\gamma_{\{(>\mathrm{Me-OH})^{-1/2}\}} C^b_{\mathrm{H}^+}\exp\left(\frac{F\zeta}{RT}\right)}, \tag{7}$$

$$\Gamma_{MAX} := \gamma_{\{(>\mathrm{Me-OH})^{-1/2}\}} + \gamma_{\{(>\mathrm{Me-OH_2})^{+1/2}\}}, \tag{8}$$

denote the equilibrium constant for complexation reaction and the maximum surface density, respectively. $\gamma_{\{(>\mathrm{Me-OH_2})^{+1/2}\}}$ and

$\gamma_{\{(>\mathrm{Me-OH})^{-1/2}\}}$ are the surface density of the complex $(>\mathrm{Me}-\mathrm{OH}_2)^{+1/2}$ and $(>\mathrm{Me}-\mathrm{OH})^{-1/2}$, respectively. $C^b_{\mathrm{H}+}$ is the local bulk concentration of hydrogen ion. F is the Faraday constant, R the gas constant and T the temperature, which is 298 K in this work.

Meanwhile, the Grahame equation gives

$$\sigma = \sqrt{8\epsilon RTC_b}\sinh\left(\frac{F\zeta}{2RT}\right). \tag{9}$$

where C_b denotes the local bulk concentration of electrolyte solution. By solving Eqs. (6) and (9) simultaneously, one obtains the values of ζ and σ.

Further, de Lima et al. [42] derived an analytical formulation of ζ as a function of C_b and pH using perturbed analysis

$$\begin{cases} \zeta = -\left[\ln h + \ln\left(1 + \frac{1-h}{h}\frac{2A\sqrt{hC_b}}{1+2A\sqrt{hC_b}}\right)\right] \\ \text{with} \quad h := \left(KC^b_{\mathrm{H}^+}\right)^{-1} = 10^{\mathrm{pH-pK}}; \quad A := \sqrt{8\epsilon RT}\Big/F\Gamma_{MAX}, \end{cases} \tag{10}$$

where pK, defined as $\log_{10}K$, is the isoelectric point.

In this paper, we use pK = 5.5 and $\Gamma_{MAX} = 3$ sites/nm^2, which is reported by de Lima et al. [40] to best fit the titration curve of Kaolinite. Once determined by experiments, other pairs of pK and Γ_{MAX} can be used. To further reduce the cost for computing local zeta potential, the analytical solution by Eq. (10) will be implemented in the algorithm other than the numerical solution to Eqs. (6) and (9). This simplification is judged by the good agreement between analytical solution and numerical solution shown in Fig. 4(a) and (b). Moreover, note that zeta potential is strongly dependent on pH while weakly dependent on concentration in present surface complexation model. Therefore, we will mainly focus on the effects of pH in the results part while put the effects of concentration aside. The readers, however, should be aware that this is not a general, but a model-dependent result.

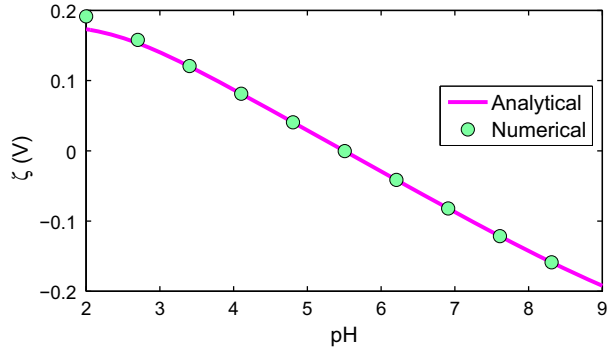

(a) zeta potential for different pH with $C_b = 1\times10^{-3}$ mol/L

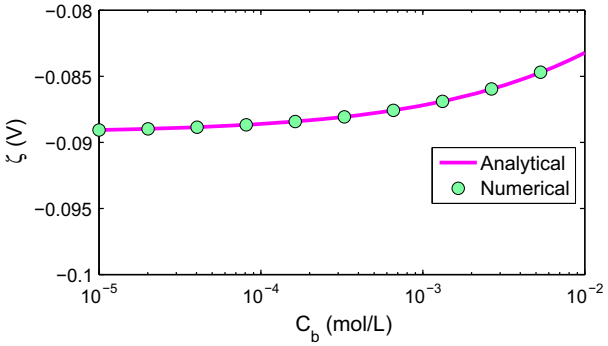

(b) zeta potential for different concentrations with pH = 7

Fig. 4. Prediction of zeta potentials for different pH and ionic concentrations using 1-pK model [41,42] with pK = 5.5. Solid line denotes the analytical solution of Eq. (10), while circle symbols denote the numerical solution of Eqs. (6) and (9).

3.3. Ionic concentration distribution

The NaCl aqueous solution considered in this work contains four kinds of major ions: Na^+, Cl^-, H^+ and OH^-. As shown in Section 3.2, the hydrogen ions and the hydroxyl ions are potential-determining ions and the zeta potential is strongly dependent on pH. The mass conservation of Na^+, Cl^-, H^+ and OH^- can be written as

$$\frac{\partial C_i}{\partial t} + \nabla\cdot\boldsymbol{J}_i = R_i, \tag{11}$$

with mass flux

$$\boldsymbol{J}_i = \boldsymbol{u}C_i - D_i\nabla C_i - z_i b_i C_i\nabla\psi \tag{12}$$

where $i = Na^+, Cl^-, H^+$ or OH^-. The right-hand-side terms in Eq. (12) represent mass transfer by convection, diffusion and electromigration, respectively. The only homogeneous reaction in this system is water ionization. R_i represents the amount of ions produced by water ionization,

$$\mathrm{H_2O} \leftrightarrow \mathrm{H^+ + OH^-}. \tag{13}$$

By assuming instantaneous equilibrium of water ionization, it leads to $C_{H^+}\times C_{OH^-} = K_w$ where $K_w = 10^{-14}$ mol^2/L^2 is the ionic product of water at 298 K [59]. The transport equation can be solved in an operator-splitting manner [60]. Firstly, Eq. (11) is solved by setting right-hand-side term to be 0. Next, C_{H^+} and C_{OH^-} are updated according to $C_{H^+}\times C_{OH^-} = K_w$. Similarly, convection-diffusion-migration equation Eq. (11) is solved for the concentration of Na^+ with $R_{Na^+} = 0$ and the concentration of Cl^- is obtained by electroneutrality.

3.4. Electrical potential field

By ignoring the magnetic effects, one can obtain the distribution of electrical potential by the Gauss's law [2],

$$\nabla\cdot(\epsilon\boldsymbol{E}) = \rho_e. \tag{14}$$

with $\boldsymbol{E} = -\nabla\psi$. Owing to the electroneutrality condition outside EDLs in the thin layer regime concerned in this work, it leads to the Poisson equation for electrical potential,

$$\nabla^2\psi = 0, \tag{15}$$

where the permittivity of the electrolyte solution ϵ is assumed to be a constant. For common mineral-electrolyte interface with a large dielectric contrast, the boundary condition at the interface for ψ is a Neumann-type boundary [61],

$$\nabla\psi\cdot\boldsymbol{n} = 0, \tag{16}$$

where $\boldsymbol{n}$ is the normal vector at the interface.

3.5. Solution strategy

The governing equations with definite conditions in Sections 3.1–3.4 can be solved as follows, no matter what numerical method is used. First, the electrical potential governed by Eq. (15) is decoupled from the ionic distribution due to

electroneutrality and can be determined independently. Eqs. (3) and (4) for fluid flow and Eq. (11) for ion concentration are coupled together. On the one hand, ionic transport is dependent on velocity field via electro-osmotic convection. On the other hand, since the zeta potential is affected by local ion distribution, the induced slip velocity and thus the electro-osmotic flow is influenced by ion transport. Consequently, we solve these two equations in an iterative way. The flow scheme of the model is as follows,

1. After initialization, solve Poisson equation, Eq. (15), for electrical potential first.
2. Solve the mass conservation equation of ions, Eq. (11), for ionic concentration C_{Na^+}, C_{H^+} and C_{OH^-}. Determine C_{Cl^-} by electroneutrality.
3. Based on the distribution of ions, calculate the local zeta potential at the surface using the 1-pK surface complexation model.
4. Solve the governing equations for fluid flow, Eqs. (3) and (4), for the velocity field with the slip velocity determined by step 3.
5. Go back to step 2 and continue the loop until convergence. (criteria for convergence: the relative error of permeability smaller than 1%).

In fact, for cases with moderate applied electrical strength, the electromigration dominates the process of ion transport. Therefore, the calculation reaches convergence quickly within finite iteration steps.

4. Numerical framework

This section presents the numerical framework, which consists of a reconstruction method for microstructure of porous media and the numerical method for solving the governing equations.

4.1. Reconstruction of porous media

In essence, the complexity of porous media comes from its irregular and random structure, and thus it plays a critical role to obtain the morphological information of the porous media. Thanks to the progress in imaging techniques, it has been made possible to extract the microscopic 3D structure of porous media such as rock samples. The resolution can reach as high as a few hundreds of nanometers with micro-CT scanning [48]. The extracted image by CT scanning needs to be filtered to provide the required binary image (i.e., solid and void) for further transport simulation. The main limitations of this procedure are two-fold. On the one hand, the high-resolution imaging techniques like micro-CT are still high-cost and time-consuming. This makes it difficult to access by academic research, especially for study on large amount of samples for comparison or to eliminate the randomness. On the other hand, the quality of final image depends on the chosen threshold values in the filtering process, which is somewhat artificial.

Apart from the imaging-based approach, another strategy is to obtain the 3D structure by computer algorithms. This algorithm-based approach provides a low-cost and convenient way to study the relation between structure and property of porous media. Various methods have been proposed. Generally, these methods can be divided into two main categories: genesis imitation method and statistical reconstruction method. The first type of the methods, genesis imitation method, consists in explicit simulation of forming processes of porous media, for example, sedimentation or cluster growth. Among the sedimentation-type method, most of them borrow ideas from packing problems to reproduce unconsolidated media [62,63]. More complicated methods, for example, the one proposed by Bakke and Øren [64] includes three reconstruction steps representing deposition, compaction and consolidation respectively. Despite that these methods are physically appealing, their use is mostly limited to packings of regularly-shaped particles and their success highly relies on the understanding of the physical processes [65].

Another type of genesis imitation method is the random generation growth method (RGG) proposed by Wang et al. [54]. Inspired by cluster growth theory, RGG method is designed to reproduce structure assembles of elements with random sizes, locations and orientations, and connections, each of which grows from a randomly distributed seeds and the growth is guided by a few given probabilistic growth rates [51]. Different types of porous structures, i.e., fibrous, granular and network, can be reconstructed by RGG [54,66,67]. Compared with the statistical reconstruction method below, RGG is a more comprehensive method with physically clear and interpretable morphological parameters (statistical information) as input.

Based on the statistical perspective, the statistical reconstruction methods generate random fields to resemble the stochastic feature of natural porous media under the constraint of low-order statistical information obtained by experiment. Among them are simulated annealing method (SA) (e.g., [68,69]) and thresholded Gaussian field method (TGF) (e.g., [70,71]). These two methods differ from each other in the low-order statistical information they use. Typically, two-point probability function and lineal-path function are adopted in SA [72,68] while void-phase autocorrelation function [71] and size distribution spectrum [73] are used in TGF.

In this work, we employ RGG method for saturated granular media, also termed as Quartet Structure Generation Set (QSGS), to reconstruct 3D microstructures of porous media, which resemble the real structure in nature like soil or clay. Fig. 5 shows the slices of generated 3D structures of granular porous media for different porosities. Other parameters such as granular size and anisotropy also can be tuned. The black parts and the white parts represent the solid phase and void space occupied by liquid respectively and the gray layers in between represent the solid-liquid boundary. Note that the original algorithm in Wang et al. [54] may generate some isolated granules and non-percolating channels, which have no contributions for ionic transport and make the solver unstable. These regions have been removed by a post-processing algorithm following the idea in Adler [74]. Therefore, the porosity in this work all refers to the effective porosity.

4.2. Lattice Boltzmann methods

Lattice Boltzmann method is a promising numerical method for simulating fluid flow and modeling multi-physical transports in fluid [55,75]. Originally proposed to make the Navier-Stokes equation solved, LBM has been extended to solve other types of partial differential equations like the convection-diffusion equation and

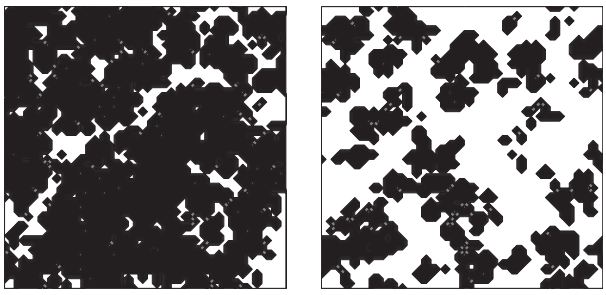

(a) porosity=0.3 (b) porosity=0.7

Fig. 5. Slices of 3D generated structures of granular porous media with a 60×60 mesh for different porosities.

the Poisson equation. There have been several successful attempts using LBM to simulate electrokinetic flow in microchannel (e.g., [76–78]) and porous media (e.g., [52,30]). Coupled lattice Boltzmann framework, proposed by Wang and Kang [79] and modified by Yoshida et al. [80], Zhang and Wang [43], has been applied to solve PNP model while Hlushkou et al. developed a hybrid framework with LBM for velocity field and finite difference [76] or random walk method [52] for transport. In this paper, we follow the modified coupled lattice Boltzmann framework to solve all the governing equations using LBM [80,43]. Present model differs from previous ones in that the slipping model is employed, other than PB model [30] or PNP model [79,80,43]. Therefore, the constraint of grid size from resolution of diffuse layer can be removed, which allows us to simulate a large system around centimeter with pore size of millimeter. In the following of this section we first give a brief introduction of the evolution equations for governing equations, then present some details about the implementation of slip velocity in LBM. Readers interested in the aspects of choice of parameters and implementation of other boundary conditions can refer to Wang and Kang [79], Zhang and Wang [81] and references therein.

4.2.1. Evolution equations

Generally, under the assumption of thin layers, i.e., the slipping model, we have to solve Eqs. (3) and (4) for velocity $\boldsymbol{u}$, Eq. (11) for C_i ($i = Na^+, H^+, OH^-$) and Eq. (15) for the local electrical potential, ψ. The corresponding lattice evolution equations for $\boldsymbol{u}, C_i$ and ψ are

$$f_\alpha(\boldsymbol{r}+c_f\delta t_f\boldsymbol{e}_\alpha,t+\delta t_f)-f_\alpha(\boldsymbol{r},t)=-\frac{1}{\tau_f}\left[f_\alpha(\boldsymbol{r},t)-f_\alpha^{eq}(\boldsymbol{r},t)\right],\quad \alpha=0-18, \tag{17}$$

$$g_{i,\alpha}(\boldsymbol{r}+c_{g_i}\delta t_g\boldsymbol{e}_\alpha,t+\delta t_g)-g_{i,\alpha}(\boldsymbol{r},t)=-\frac{1}{\tau_g}\left[g_{i,\alpha}(\boldsymbol{r},t)-g_{i,\alpha}^{eq}(\boldsymbol{r},t)\right],\quad \alpha=0-6, \tag{18}$$

$$h_\alpha(\boldsymbol{r}+c_h\delta t_h\boldsymbol{e}_\alpha,t+\delta t_h)-h_\alpha(\boldsymbol{r},t)=-\frac{1}{\tau_h}\left[h_\alpha(\boldsymbol{r},t)-h_\alpha^{eq}(\boldsymbol{r},t)\right],\quad \alpha=0-6, \tag{19}$$

where $f_\alpha, g_{i,\alpha}$ and h_α represent the distribution functions for density, concentration of ith ion and electrical potential, respectively, which are functions of position vector $\boldsymbol{r}$, time t and discrete unit direction vector $\boldsymbol{e}_\alpha$. $[c_f,\tau_f,\delta t_f],[c_{g_i},\tau_{g_i},\delta t_{g_i}]$ and $[c_h,\tau_h,\delta t_h]$ are the corresponding dimensional lattice speed, dimensionless relaxation time and dimensional time step for each evolution equation. Note that we employ a $D3Q19$ model to solve the velocity field for higher accuracy with convection term, while use a $D3Q7$ model for both concentration and electrical potential fields for higher stability and efficiency in because of absent convection terms in the corresponding governing equations. The dimensional lattice speeds c_f, c_{g_i} and c_h are independent from each other, and thus can be tuned to improve the efficiency and stability with the constraint that τ_f, τ_{g_i} and τ_h in the range of $[0.5, 2]$ [67].

For solving the velocity field, the density equilibrium distribution function f_α^{eq} takes the form

$$f_\alpha^{eq}=\omega_\alpha\rho\left[1+3\frac{\boldsymbol{e}_\alpha\cdot\boldsymbol{u}}{c_f}+9\frac{(\boldsymbol{e}_\alpha\cdot\boldsymbol{u})^2}{2c_f^2}-\frac{3\boldsymbol{u}^2}{2c_f^2}\right], \tag{20}$$

with the discrete unit direction vectors

$$\boldsymbol{e}_\alpha=\begin{cases}(0,0,0), & \alpha=0\\ (\pm1,0,0),(0,\pm1,0),(0,0,\pm1), & \alpha=1-6\\ (\pm1,\pm1,0),(\pm1,0,\pm1),(0,\pm1,\pm1), & \alpha=7-18\end{cases} \tag{21}$$

and the distribution coefficients $\omega_\alpha=1/3,\alpha=0;\omega_\alpha=1/18,\alpha=1-6;\omega_\alpha=1/36,\alpha=7-18$. In $D3Q19$ model, $\tau_f=\frac{3\nu}{c_f\delta x}+0.5$ where δ_x is the grid size and ν the kinematic viscosity of fluid.

For solving the ionic concentration and electrical potential field, the equilibrium distribution functions are

$$g_{i,\alpha}^{eq}=\overline{\omega}_\alpha C_i\left[1+3\frac{\boldsymbol{e}_\alpha\cdot(\boldsymbol{u}-z_ib_i\nabla\psi)}{c_{g_i}}\right], \tag{22}$$

$$h_\alpha^{eq}=\overline{\omega}_\alpha\psi, \tag{23}$$

with the discrete unit direction vectors

$$\boldsymbol{e}_\alpha=\begin{cases}(0,0,0), & \alpha=0\\ (\pm1,0,0),(0,\pm1,0),(0,0,\pm1), & \alpha=1-6\end{cases} \tag{24}$$

and the distribution coefficients $\overline{\omega}_\alpha=1/4,\alpha=0;\overline{\omega}_\alpha=1/8,\alpha=1-6$. In $D3Q7$ model, $\tau_{g_i}=\frac{4D_i}{c_{g_i}\delta x}$ where D_i is the diffusivity of ith ion. For electrical potential, $\tau_h=\frac{4}{c_h\delta x}$.

The macroscopic quantities can calculated as

$$\rho=\sum_{\alpha=0}^{18}f_\alpha, \tag{25}$$

$$\rho\boldsymbol{u}=\sum_{\alpha=0}^{18}\boldsymbol{e}_\alpha f_\alpha, \tag{26}$$

$$C_i=\sum_{\alpha=0}^{6}g_{i,\alpha}, \tag{27}$$

$$\psi=\sum_{\alpha=0}^{6}h_\alpha. \tag{28}$$

4.2.2. Implementation of slip velocity

The main numerical issue for slipping model is to implement the slip velocity on the boundary in LBM. The basic idea here follows the one proposed by Ladd [82] for dealing with moving solid–fluid boundary conditions in particle suspension. Essentially, Ladd's method can be seen as a modified bounceback method including a term accounting for the velocity on the boundary. The unknown post-collision distribution function $\tilde{f}$ of each link can be determined as

$$\tilde{f}_{\alpha'}=f_\alpha+\frac{6\omega_\alpha\rho}{c_f}(\boldsymbol{e}_{\alpha'}\cdot\boldsymbol{u}_b) \tag{29}$$

where ρ is the local density and $\boldsymbol{e}_{\alpha'}$ and $\boldsymbol{e}_\alpha$denote the inward direction vector pointing to the liquid phase and outward direction vector pointing to the solid phase respectively. The boundary velocity, $\boldsymbol{u}_b$, is determined by HS equation and in parallel with the local boundary. As shown in Fig. 6, the liquid cell O in the corner is connected with solid cell P and Q by face Γ_{OP} and Γ_{OQ}. The slip velocity at the boundaries are denoted as $u_{b,z}$ and $u_{b,y}$. However, if we perform Eq. (29) to compute the unknown distribution function for $\alpha=5$, there is a subtle issue to determine the boundary velocity at point x_5 since it is actually a singular point generated by the stair-wise geometry. (Note that in particle suspension problem, $\boldsymbol{u}_b$ at x_5 is determined by particle motion independent of the boundary geometry, and thus there is no such singularity issue.) Another problem of this link-based scheme is that it is not necessarily mass-conservative. To overcome these problems, we propose a face-based scheme, which is mass-conservative and more consistent with the surface induced velocity in electro-osmosis.

We illustrate the procedure using a 2D case shown in Fig. 6 and it can be applied to 3D case easily. First we choose a liquid cell on

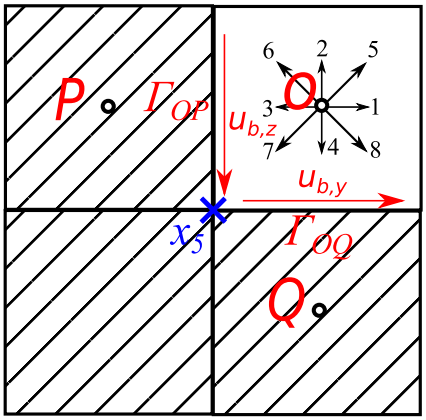

Fig. 6. Illustration for implementing face-based slip velocity boundary in LBM. Liquid cell O is connected with solid cell P and Q by face Γ_{OP} and Γ_{OQ}. Slip velocities $u_{b,y}$ and $u_{b,z}$ determined by HS equation live on Γ_{OP} and Γ_{OQ}.

the boundary, i.e., O here. Then search around O in the main direction $1, 2, 3, 4$ to determine how many solid–liquid boundaries it has. In this case, there are two denoted by Γ_{OP} and Γ_{OQ}. Next, for each solid–liquid boundary, use Eq. (29) to obtain the unknown distribution functions with the boundary related velocity $\boldsymbol{u}_b$. Take Γ_{OQ} as an example, $\tilde{f}_6$ is calculated as $\tilde{f}_6 = f_8 - \frac{6\omega_\alpha \rho}{c_f} u_{b,y}$ and $\tilde{f}_2 = f_4$ since $\boldsymbol{e}_2$ is normal to the velocity $u_{b,y}$. Note that in this case, $\tilde{f}_5$ should be updated twice for both Γ_{OP} and Γ_{OQ}, and the contributions are added together.

5. Results and discussion

In this section, we present the simulation results of inhomogeneously charged electro-osmosis in 3D granular porous media. Fig. 7 shows a typical porous structure used in simulation with length $L = 10$ cm and a square cross-section. The system includes Na^+, H^+, OH^- and Cl^-. At the inlet and outlet boundary, concentrations of ions, pH, pressure and electrical potential are fixed, while the lateral boundaries are periodic. Typically, the concentration of Na^+ is fixed as 10^{-3} mol/L at both inlet and outlet. Physical parameters are given in Table 1. To meet the requirement for representative elementary volume (REV), we employ a mesh of $100 \times 30 \times 30$ so that the ratio of number of grids on one side (i.e.,30 for y- or z-axis and 100 for x-axis) over number of granules with the characteristic size is generally larger than 10.

Table 1
Physical parameters in the simulation.

Physical meaning	Symbol	Value
Density of electrolyte solution	ρ	999.9 Kg/m^3
Kinematic viscosity of electrolyte solution	ν	0.89×10^{-6} Pa s
Permittivity of electrolyte solution	ϵ	6.95×10^{-10} F/m
Diffusivity of H^+	D_{H^+}	9.3×10^{-9} m^2/s
Diffusivity of OH^-	D_{OH^-}	5.3×10^{-9} m^2/s
Diffusivity of Na^+	D_{Na^+}	1.3×10^{-9} m^2/s
Diffusivity of Cl^-	D_{Cl^-}	2.0×10^{-9} m^2/s

In this work, the electro-osmotic permeability in the main direction (i.e., x-direction) is defined as

$$\kappa_e = \frac{\langle u_x \rangle}{\langle E_x \rangle}, \tag{30}$$

where $\langle \cdot \rangle = \frac{1}{V} \int_V dV$ means average over the total volume. Therefore, it follows that $\langle u_x \rangle$ represents the macroscopic electro-osmotic velocity (electro-osmotic velocity for short) and $\langle E_x \rangle$ is equal to the macroscopic electrical field, $-\frac{\Delta\psi}{L}$ (see Appendix B), where $\Delta\psi$ is electrical potential difference between inlet and outlet. In the following, we will drop the subscript x as we only talk about the transport in the main direction.

5.1. Comparison with macroscopic model

Under the assumption of thin double layer and negligible surface conductance, Overbeek [83] has given a relation to determine electro-osmotic permeability based on the ratio of to the conductivity of the porous media to the electrolyte conductivity,

$$\kappa_e = -\frac{\epsilon\zeta}{\mu}\left(\frac{K}{K_f}\right), \tag{31}$$

where K and K_f are the conductivity of the porous media and the electrolyte conductivity, respectively. We give a derivation of Eq. (31), see Appendix B. The ratio can be related to tortuosity and porosity as [84]

$$\frac{K}{K_f} = \frac{\phi}{\tau^2}, \tag{32}$$

where τ is the tortuosity. As a result, Eq. (31) can be written as

$$\kappa_e = -\frac{\epsilon\zeta}{\mu}\left(\frac{\phi}{\tau^2}\right). \tag{33}$$

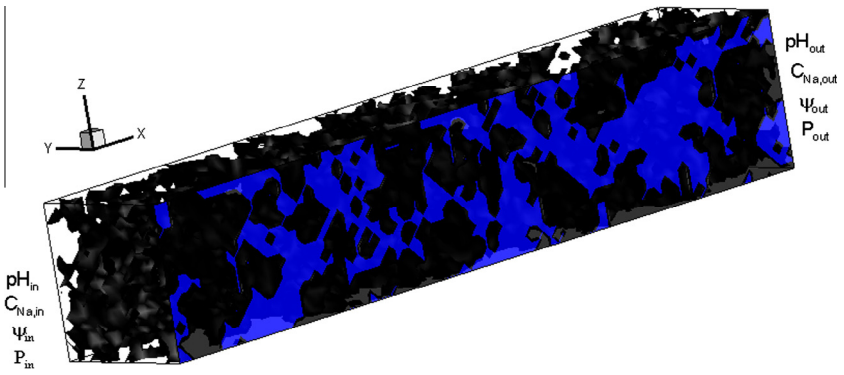

Fig. 7. Schematic of 3D granular porous media generated by RGG method [54] for electro-osmotic simulation with black part representing solid and blue part representing liquid. X-axis indicates the main direction of electro-osmotic flow. Concentration of ions, pH, pressure and electrical potentials are fixed at inlet and outlet.

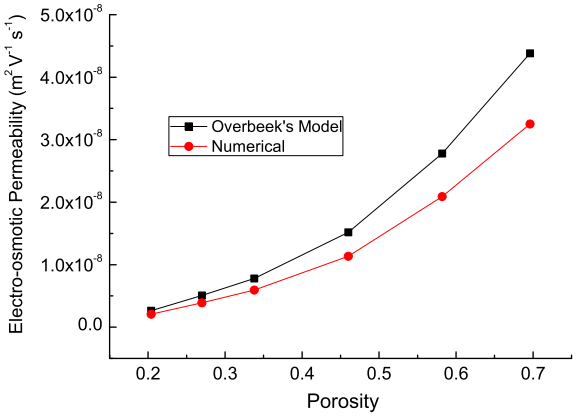

Fig. 8. Comparison of electro-osmotic permeability given by Overbeek's model and numerical simulation for homogeneously charged granular porous media with pH = 8. Black symbols represent values calculated by Eq. (33) while red symbols represent values obtained by our numerical method. Samples with $100 * 30 * 30$ mesh are generated by RGG method for different porosities.

In order to evaluate tortuosity, Johnson et al. [85] gives an analytical approach using the solution of potential flow. Based on this, Pride [61][1] shows that tortuosity can be calculated as

$$\tau^2 = \frac{\langle E \rangle}{\langle E \rangle_p}, \tag{34}$$

where $\langle \cdot \rangle = \frac{1}{V_p} \int_{V_p} dV$ is the average over the pore space or liquid phase. V_p means the volume of pore space.

In Fig. 8, we compare electro-osmotic permeability by Overbeek's model and numerical simulation for homogeneously charged granular porous media with pH = 8. In consideration of the randomness of porous media, the agreement is good, which indicates the validity of our algorithm. In fact, the assumption of similitude between velocity and electrical field in Overbeek's model can not be fully satisfied in our case,especially at the inlet and outlet (necessary condition for this similitude can refer to Cummings et al. [87]), which might be the reason for the difference at large porosity.

5.2. Nonlinear response of inhomogeneously charged electro-osmosis

Numerous works on electro-osmosis with homogeneous charge have shown that the electro-osmotic permeability is only related to the structure and surface property of the porous media, but irrelevant to the external electrical field. In fact, this is to say, the electro-osmotic velocity is linearly related to the external electrical field, which is intrinsically assumed by using linear phenomenological relations. However, when the surface is inhomogeneously charged, this obvious property may not be valid. One macroscopic evidence for this nonlinear effect is in the study of electrokinetic remediation. Reverse electro-osmotic flow has been observed (e.g., [36]), which indicates a change of sign of the electro-osmotic permeability. Inspired by previous study, we attempt to investigate this nonlinear effect in porous media by simulation. Because of the weak dependence of the zeta potential on the concentration in our 1-pK model (see Fig. 4(b)), we will focus on the effect of inhomogeneous pH.

Firstly, a pH difference is imposed to induce an inhomogeneous distribution of surface charge on the porous structure. To be specific, different pH values are assigned at the inlet and outlet in Fig. 7, which correspond to Dirichlet boundary conditions for transport of H^+ and OH^-. The steady state distribution of pH is generally nonlinear and dependent on the external electrical field, as shown in Fig. 10 for inlet pH = 6 and outlet pH = 8. Under the same condition, the black curve in Fig. 9 illustrates the electro-osmotic velocity for different applied electrical strengths. When E is smaller than 20 V/m, the electro-osmotic velocity shows a nonlinear response to the increase of the electrical field strength. The reason is that increase of electrical field will have different effects on H^+ and OH^- because of the difference of electrical mobility. Specifically, since the diffusivity, thus the electrical mobility, of H^+ is larger than that of OH^-, when the electrical field increases, the hydrogen front will move to the outlet (the cathode end). As a result, the distribution of pH is affected by the applied electrical field (see Fig. 10). According to the ζ - pH curve in Fig. 4(a), decrease of pH from 8 to 6 will reduce the absolute value of zeta potential. Therefore, the total effect of increasing E on electro-osmotic velocity will be partly counterbalanced by the decrease of $|\zeta|$, which leads to a nonlinear dependence. In terms of electro-osmotic permeability, different from homogeneous charge case, where it is a constant, the electro-osmotic permeability is generally dependent on the applied electrical field in inhomogeneous charge case. However, when E is large enough, the electrical force will be dominant in the distribution of potential-determining ions and the pH distribution doesn't change much in this situation. Consequently, the electro-osmotic velocity grows linearly with applied electrical field strength.

When the inlet and outlet pH are fixed as 5 and 9, the blue[2] line in Fig. 9 shows that the electro-osmotic velocity will have a dramatical change of direction with the increase of electrical field strength. When E is about 25 V/m, flow reverses. The reason is that the isoelectric point of the porous material, pK = 5.5, is above the inlet pH, and hence part of the surface is positively charged, which leads to a local reverse flow. When E is small, the positive charge only occupy a small portion of the system near the inlet and the reverse flow is overwhelmed by the forward main stream. As the electrical field increases, it pushes the hydrogen front to the outlet. As a result, the area of positive charge expands and leads to a dominant reverse flow as a whole. Further increase of electrical field induces a linear increase of the magnitude of electro-osmotic velocity since the electrical force dominates as before.

This nonlinearity comes from the fact that the electrical field affects not only the slip velocity by HS equation, but also the distribution of potential-determining ions, which is a feature of inhomogeneous charge. In our case, since the potential-determining ions are H^+ and OH^-, the distribution of pH plays a key role. When the electrical force dominates the transport process over convection and diffusion, the nonlinear effect vanishes and electro-osmotic permeability will be a constant. In addition, the reverse of flow is closely related to the isoelectric point and it emerges when the positively charged area is dominant in the whole system.

Furthermore, we investigate inhomogeneously charged electro-osmosis in different pH regimes and porosities to figure out when is the nonlinear effect important. Fig. 11 shows electro-osmotic permeability with homogeneous charge and inhomogeneous charge for (a) acidic (pH = 3–5) and (b) nearly neutral (pH = 6–8) and (c) alkaline (pH = 7–9) conditions with porosity ranging from 0.2 to 0.7. The given electro-osmotic permeabilities are averaged over two different samples with same statistical geometrical feature and the standard deviation of the electro-osmotic permeability is also shown in the figure as the error bar.

[1] Tortuosity in Pride's paper actually means square of tortuosity here. This conceptual confusion has been explained by Epstein [86].

[2] For interpretation of color in 'Fig. 9', the reader is referred to the web version of this article.

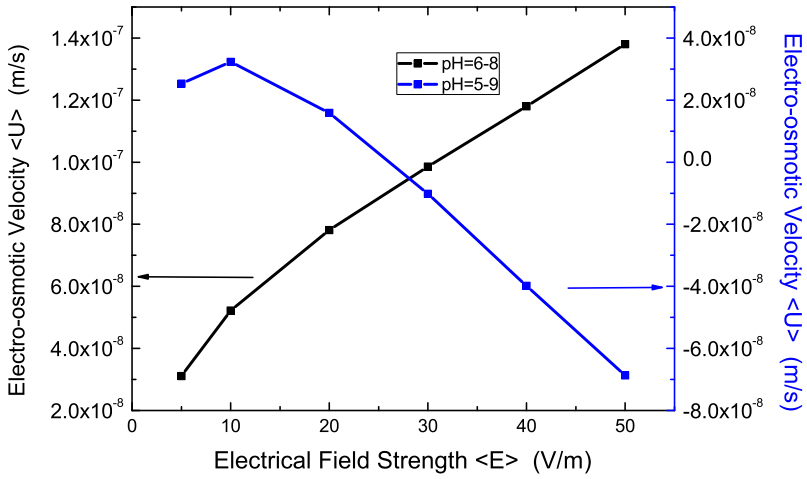

Fig. 9. Macroscopic electro-osmotic velocity for different applied electrical strengths with $pH_{in} = 6$ and $pH_{out} = 8$ (left-y) or $pH_{in} = 5$ and $pH_{out} = 9$ (right-y). The porosity of this sample is 0.46.

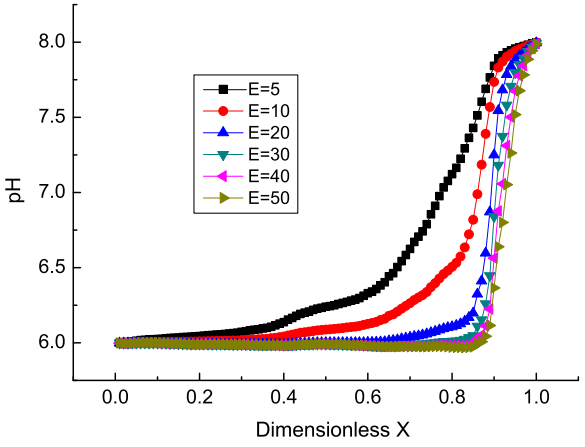

Fig. 10. Profiles of cross-section averaged pH along the x-direction for different applied electrical strengths with $pH_{in} = 6$ and $pH_{out} = 8$. The porosity of this sample is 0.46. Symbols with different colors represent results for different macroscopic electrical strength $E = 5, 10, 20, 30, 40, 50$ V/m. (For interpretation of the references to color in this figure legend, the reader is referred to the web version of this article.)

Clearly, for all cases, the electro-osmotic permeability of homogeneous charge sets upper and lower bounds for that of inhomogeneous charge. For pH = 3–5, the solid/liquid interface is positively charged so that reverse flow is induced and electro-osmotic permeability is negative. What's more, comparison with cases with homogeneous charge demonstrates that the nonlinear response, or dependence on electrical field is most noticeable for nearly neutral cases ($pH = 6 - 8$). In the pH range from 3 to 5, H^+ is dominant in most part of the pore space while OH^- dominates for pH from 7 to 9. Under both circumstances, the influence of electrical field on pH distribution is relatively small, and therefore the electro-osmotic permeability of inhomogeneous charge is closer to the that of homogeneous charge. In terms of porosity, there is a similar trend for both homogeneous cases and inhomogeneous charge cases. In addition, this strong influence of porosity on the electro-osmotic permeability has been observed in Wang and Chen [30] which employs a Poisson–Boltzmann model.

6. Conclusions

In this contribution, we first propose a quantitative criteria for classifying electro-osmosis based on a dimensionless number M, which is the ratio of Debye length and characteristic pore size. This classification, on the one hand, can be used as a guideline for simplification of electro-osmotic model. On the other hand, we attempt to follow the spirit of this classification to overcome the difficulty from the problematic definition for "local bulk property", which plays a key role in inhomogeneously charged electro-osmosis.Following this classification, we can focus on the simplest case, the thin-layer regime ($M < 0.01$) in this work. Based on numerical reconstruction method and LBM solver, we simulate the electro-osmosis using the pore-scale slipping model. Present results show that for small electrical field strength, the effect of electrical force on distribution of pH gives rise to the nonlinear response. In an extreme case with inlet pH smaller than the isoelectric point, a reversal of flow occurs with increase of electrical field. Moreover, this nonlinear feature is most noticeable for nearly pH-neutral region since H^+ and OH^- are competing in this situation, which needs to be validated by further experimental data. More complicated regimes with electrical double layer overlap will be studied in our future work.

Acknowledgements

The authors are grateful to Dr. Hlushkou, Dr. Y. Chen, Dr. L. Chen and Prof. Andre Revil for helpful discussions. This work is financially supported by the NSF grant of China (No. 51676107 and 51176089) and the National Science and Technology Major Project on Oil and Gas (No. 2017ZX05013001).

Appendix A. Correction factor

First, we define the dimensionless length $l^* = \frac{l}{\lambda_D}$, which is the reciprocal of the dimensionless Debye length M. l^* is also called electrokinetic radius in [23]. Similarly, y^* is defined as $\frac{y}{\lambda_D}$. When there is no overlap of EDL, the analytical solution for PB equation of 1:1 type electrolyte takes the following form

$$\psi^* = 4\tanh^{-1}\left(\tanh\left(\frac{\zeta^*}{4}\right)\exp\left(-\frac{l^*}{2} + |y^*|\right)\right) \tag{A.1}$$

Because of the similitude of velocity and electrical field,

$$u = -\frac{\epsilon E_{ext}}{\mu}(\psi - \zeta). \tag{A.2}$$

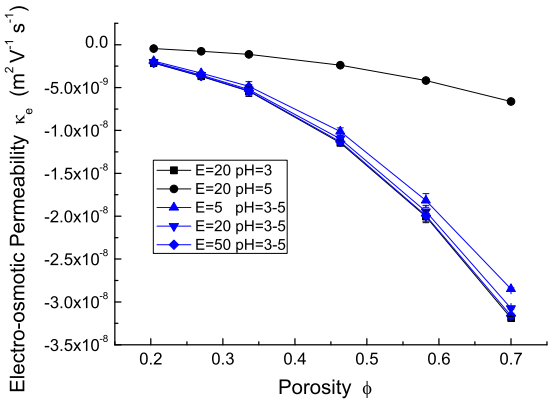

(a) homogeneous charge (pH=3 and pH=5) and inhomogeneous charge (pH=3-5)

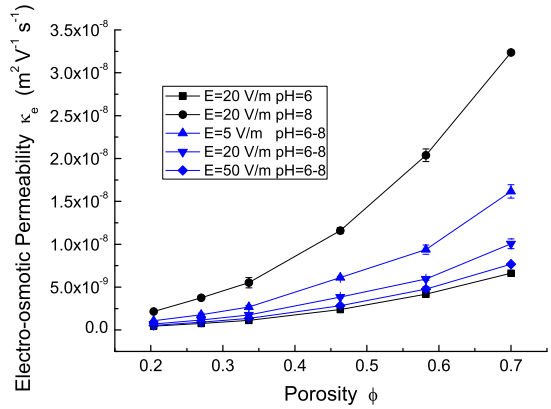

(b) homogeneous charge (pH=6 and pH=8) and inhomogeneous charge (pH=6-8)

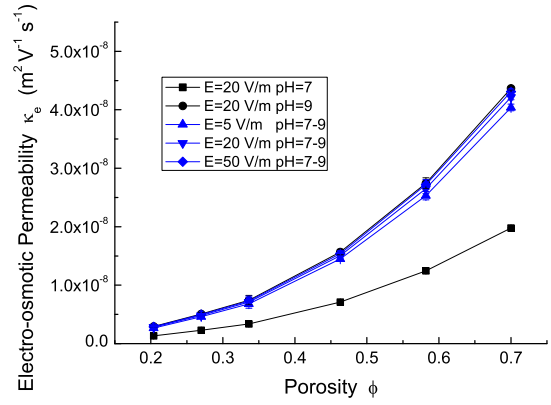

(c) homogeneous charge (pH=7 and pH=9) and inhomogeneous charge (pH=7-9)

Fig. 11. For porosity ranging from 0.2 to 0.7, electro-osmotic permeability with homogeneous charge and inhomogeneous charge for (a) acidic (pH = 3–5) and (b) nearly neutral (pH = 6–8) and (c) alkaline (pH = 7–9) conditions. Black symbols represent cases with homogeneous charge while blue ones represent cases with inhomogeneous charge. (For interpretation of the references to color in this figure legend, the reader is referred to the web version of this article.)

The correction factor is defined as

$$\Theta = \frac{U_{avg}}{U_{HS}} = \frac{\int_{-\frac{l^*}{2}}^{\frac{l^*}{2}} u dy^*}{U_{HS}}. \tag{A.3}$$

Substitute Eqs. (A.1) and (A.2) into Eq. (A.3), the correction factor can be written as

$$\Theta = \frac{1}{l^*}\int_{-\frac{l^*}{2}}^{\frac{l^*}{2}} \left[1 - \frac{4}{\zeta^*}\tanh^{-1}\left(\tanh\left(\frac{\zeta^*}{4}\right)\exp(-\frac{l^*}{2} + |\, y^*\,|)\right)\right] dy^*. \tag{A.4}$$

Thanks to the symmetry, the domain of integration can be replaced by $[0, \frac{l^*}{2}]$ through multiplying a factor of 2 and after some simplification, Eq. (A.4) is written as

$$\Theta = 1 - \frac{8}{\zeta^* l^*}\int_0^{\frac{l^*}{2}} \tanh^{-1}\left(\tanh\left(\frac{\zeta^*}{4}\right)\exp\left(-\frac{l^*}{2} + y^*\right)\right) dy^*. \tag{A.5}$$

Therefore, the main difficulty to give a analytical form for Θ lies in simplifying the integration which can be defined as

$$I(\zeta^*, l^*) = \int_0^{\frac{l^*}{2}} \tanh^{-1}\left(\frac{\zeta^*}{4}\right)\exp\left(-\frac{l^*}{2} + y^*\right) dy^*. \tag{A.6}$$

It is easy to see that I is a function of dimensionless zeta potential ζ^* and dimensionless length l^*. Furthermore, we substitute z^* for $y - \frac{l^*}{2}$ and define $A = \tanh\left(\frac{\zeta^*}{4}\right)$. Then, the integral is written as follow,

$$I(A, l^*) = \int_{-\frac{l^*}{2}}^{0} \tanh^{-1}(A\exp(z^*)) dz^*. \tag{A.7}$$

When A is small, $\tanh^{-1}(x)$ can be approximated by $\tanh^{-1}(x) \approx x$. So,[3]

$$I = \int_{-\frac{l^*}{2}}^{0} (A\exp(z^*)) dz^* = A\exp(z^*)|_{-\frac{l^*}{2}}^{0} \approx A, \tag{A.8}$$

where we have used the fact that $\frac{l^*}{2} \in [5, 50]$.

Therefore, the correction factor Θ has this simple form,

$$\Theta = 1 - \frac{8}{\zeta^* l^*}\tanh\left(\frac{\zeta^*}{4}\right). \tag{A.9}$$

Fig. 3 shows the comparison between analytical result and the result from numerically integration. Generally, Eq. (2) will overestimate the correction factor because of the approximation of small A.

When ζ^* is below 1, $A = \tanh\left(\frac{\zeta^*}{4}\right) \approx \frac{\zeta^*}{4}$. Then $\Theta = 1 - \frac{2}{l^*}$, which is same with the result directly derived from Debye-Huckel approximation. When ζ^* is above 8, A will be rather close to unity and with numerical integration, we have[4]

$$I(A = 1) = \int_{-\frac{l^*}{2}}^{0} \tanh^{-1}(\exp(z^*)) dz^* \approx 1.25. \tag{A.10}$$

Therefore, Θ can be approximated by $1 - \frac{10}{\zeta^* l^*}$.

Appendix B. Derivation of macroscopic model

Though the derivation can be found in many papers or books, the author feels it necessary to give a more rigorous version as the existing derivation is either unclear or conceptually problematic. We start the derivation by defining the effect conductivity of the porous media as

$$\langle j \rangle = K\langle E \rangle, \tag{B.1}$$

where j is the electric current and E is the electrical strength. Since the solid is non-conducting, the total current $\langle j \rangle$ can be written as

$$\langle j \rangle = \frac{1}{V}\int_{V_p} j dV = \frac{K_f}{V}\int_{V_p} E dV, \tag{B.2}$$

[3] It can be further proved that A is the first-order approximation for the integral by expanding I as Taylor series.

[4] This improper integral can be proved to be convergent.

where V_p is the pore volume and K_f is the conductivity of the electrolyte solution. In the second equality above, we have used the Ohm's law in the pore space, i.e., $j = K_f E$, which is valid in the bulk electroneutral region when there is no concentration gradient. (This can be derived from the Nernst-Planck equation, see [88].) Compare Eqs. (B.1) and (B.2), we have

$$\frac{1}{V}\int_{V_p} E\,dV = \frac{K}{K_f}\langle E\rangle. \tag{B.3}$$

The macroscopic electro-osmotic velocity can be calculated as

$$\langle u\rangle = \frac{1}{V}\int_V u\,dV = \frac{1}{V}\int_{V_p} u\,dV = \frac{1}{V}\int_{V_p} -\frac{\epsilon\zeta}{\eta}E\,dV. \tag{B.4}$$

In the last equality above, we have used the Helmholtz-Smoluchowski's formula $u = -\frac{\epsilon\zeta}{\eta}E$ for the whole pore space outside EDL by assuming the similitude between velocity field u and electrical field E. Finally, by substituting Eq. (B.3) into Eq. (B.4), it leads to

$$\langle u\rangle = -\frac{\epsilon\zeta}{\eta}\frac{K}{K_f}\langle E\rangle. \tag{B.5}$$

Therefore, compared with definition Eq. (30), the macroscopic model, Eq. (31), is obtained.

Moreover, one can simply prove $\langle E\rangle = -\frac{\nabla\psi}{L}$ by expressing the averaged electrical strength vector as

$$\langle \boldsymbol{E}\rangle = \frac{1}{V}\left(\int_{\mathcal{V}_f} \boldsymbol{E}_f\,dV + \int_{\mathcal{V}_s} \boldsymbol{E}_s\,dV\right), \tag{B.6}$$

where $\boldsymbol{E}_f$ and $\boldsymbol{E}_s$ represents electrical field in fluid region $\mathcal{V}_f$ and solid region $\mathcal{V}_s$, respectively. By noticing that both $\boldsymbol{E}_f$ and $\boldsymbol{E}_s$ satisfy the Laplace equation and interchanging the integral and nabla operator, we can obtain

$$\nabla\cdot\langle \boldsymbol{E}\rangle = 0. \tag{B.7}$$

For the macroscopically 1D problem, solution to Eq. (B.7) is a constant electrical field, namely, $\langle E\rangle = -\frac{\nabla\psi}{L}$.

References

[1] K.P. Tikhomolova, Electro-osmosis, Ellis Horwood, New York, 1993.
[2] D. Li, Electrokinetics in Microfluidics, Academic, Oxford, 2004.
[3] F. Reuss, Sur un nouvel effet de l'electricite galvanique, Mem. Soc. Imperiale NaturNatural Moscou 2 (1809) 327–337.
[4] A. Mahmoud, J. Olivier, J. Vaxelaire, A.F. Hoadley, Electrical field: a historical review of its application and contributions in wastewater sludge dewatering, Water Res. 44 (2010) 2381–2407.
[5] A.S. Rathore, C. Horvth, Capillary electrochromatography: theories on electroosmotic flow in porous media, J. Chromatogr. A 781 (1997) 185–195.
[6] B.A. Grimes, A.I. Liapis, Modeling and analysis of the electrokinetic mass transport and adsorption mechanisms of a charged adsorbate in capillary electrochromatography systems employing charged nonporous adsorbent particles, J. Colloid Interf. Sci. 234 (2001) 223–243.
[7] W.R. Bowen, R.A. Clark, Electro-osmosis at microporous membranes and the determination of zeta-potential, J. Colloid Interf. Sci. 97 (1984) 401–409.
[8] Y.B. Acar, A.N. Alshawabkeh, Principles of electrokinetic remediation, Environ. Sci. Technol. 27 (1993) 2638–2647.
[9] A.P. Shapiro, R.F. Probstein, Removal of contaminants from saturated clay by electroosmosis, Environ. Sci. Technol. 27 (1993) 283–291.
[10] S. Yao, J.G. Santiago, Porous glass electroosmotic pumps: theory, J. Colloid Interf. Sci. 268 (2003) 133–142.
[11] M.Z. Bazant, T.M. Squires, Induced-charge electrokinetic phenomena, Curr. Opin. Colloid Interf. Sci. 15 (2010) 203–213.
[12] H. Daiguji, P. Yang, A.J. Szeri, A. Majumdar, Electrochemomechanical energy conversion in nanofluidic channels, Nano Lett. 4 (2004) 2315–2321.
[13] M. Wang, Q. Kang, Electrochemomechanical energy conversion efficiency in silica nanochannels, Microfluid. Nanofluid. 9 (2009) 181–190.
[14] S.J. Kim, S.H. Ko, K.H. Kang, J. Han, Direct seawater desalination by ion concentration polarization, Nat. Nanotechnol. 5 (2010) 297–301.
[15] R. Schoch, J. Han, P. Renaud, Transport phenomena in nanofluidics, Rev. Mod. Phys. 80 (2008) 839–883.
[16] A. Revil, L.M. Cathles, S. Losh, J.A. Nunn, Electrical conductivity in shaly sands with geophysical applications, J. Geophys. Res.: Solid Earth 103 (1998) 23925–23936.
[17] A. Revil, H. Schwaeger, L.M. Cathles, P.D. Manhardt, Streaming potential in porous media: 2. Theory and application to geothermal systems, J. Geophys. Res.: Solid Earth 104 (1999) 20033–20048.
[18] M. Rosanne, M. Paszkuta, J.-F. Thovert, P.M. Adler, Electro-osmotic coupling in compact clays, Geophys. Res. Lett. 31 (2004) L18614.
[19] A. Revil, A. Jardani, The Self-potential Method: Theory and Applications in Environmental Geosciences, Cambridge University Press, 2013.
[20] J. Lyklema, Electrokinetics after Smoluchowski, Colloids Surf. A 222 (2003) 5–14.
[21] R.W. O'Brien, Electroosmosis in porous materials, J. Colloid Interf. Sci. 110 (1986) 477–487.
[22] J.T.G. Overbeek, P.W.O. Wijga, On electro-osmosis and streaming-potentials in diaphragms, Recl. Trav. Chim. Pays-Bas 65 (1946) 556–563.
[23] D. Burgreen, F.R. Nakache, Electrokinetic flow in ultrafine capillary slits, J. Phys. Chem. 68 (1964) 1084–1091.
[24] C.L. Rice, R. Whitehead, Electrokinetic flow in a narrow cylindrical capillary, J. Phys. Chem. 69 (1965) 4017–4024.
[25] S. Levine, J.R. Marriott, G. Neale, N. Epstein, Theory of electrokinetic flow in fine cylindrical capillaries at high zeta-potentials, J. Colloid Interf. Sci. 52 (1975) 136–149.
[26] C. Picallo, S. Gravelle, L. Joly, E. Charlaix, L. Bocquet, Nanofluidic osmotic diodes: theory and molecular dynamics simulations, Phys. Rev. Lett. 111 (2013) 244501.
[27] A. Revil, P. Leroy, Constitutive equations for ionic transport in porous shales, J. Geophys. Res.: Solid Earth 109 (2004) B03208.
[28] M.D. Jackson, E. Leinov, On the validity of the thin and thick double-layer assumptions when calculating streaming currents in porous media, Int. J. Geophys. 2012 (2012) 1–12.
[29] D. Coelho, M. Shapiro, J.F. Thovert, P.M. Adler, Electroosmotic phenomena in porous media, J. Colloid Interf. Sci. 181 (1996) 169–190.
[30] M. Wang, S. Chen, Electroosmosis in homogeneously charged micro- and nanoscale random porous media, J. Colloid Interf. Sci. 314 (2007) 264–273.
[31] J.L. Anderson, W. Keith Idol, Electroosmosis through pores with nonuniformly charged walls, Chem. Eng. Commun. 38 (1985) 93–106.
[32] A. Ajdari, Electro-osmosis on inhomogeneously charged surfaces, Phys. Rev. Lett. 75 (1995) 755–758.
[33] A. Szymczyk, H. Zhu, B. Balannec, Pressure-driven ionic transport through nanochannels with inhomogeneous charge distributions, Langmuir 26 (2010) 1214–1220.
[34] C. Selvey, H. Reiss, Ion transport in inhomogeneous ion exchange membranes, J. Membr. Sci. 23 (1985) 11–27.
[35] G.R. Eykholt, D.E. Daniel, Impact of system chemistry on electroosmosis in contaminated soil, J. Geotech. Eng. 120 (1994) 797–815.
[36] K. Beddiar, T. Fen-Chong, A. Dupas, Y. Berthaud, P. Dangla, Role of pH in electro-osmosis: experimental study on NaCl-water saturated kaolinite, Transp. Porous Media 61 (2005) 93–107.
[37] A.N. Alshawabkeh, Y.B. Acar, Electrokinetic remediation. II: Theoretical model, J. Geotech. Eng. 122 (1996) 186–196.
[38] A.Z. Al-Hamdan, K.R. Reddy, Electrokinetic remediation modeling incorporating geochemical effects, J. Geotech. Geoenviron. Eng. 134 (2008) 91–105.
[39] T. Lemaire, C. Moyne, D. Stemmelen, Modelling of electro-osmosis in clayey materials including pH effects, Phys. Chem. Earth 32 (2007) 441–452.
[40] S.A. de Lima, M.A. Murad, C. Moyne, D. Stemmelen, A three-scale model for pH-dependent steady flows in 1:1 clays, Acta Geotech. 3 (2008) 153–174.
[41] S.A. de Lima, M.A. Murad, C. Moyne, D. Stemmelen, A three-scale model of pH-dependent flows and ion transport with equilibrium adsorption in kaolinite clays: I. Homogenization analysis, Transp. Porous Media 85 (2010) 23–44.
[42] S.A. de Lima, M.A. Murad, C. Moyne, D. Stemmelen, C. Boutin, A three-scale model of pH-dependent flows and ion transport with equilibrium adsorption in kaolinite clays: II. Effective-medium behavior, Transp. Porous Media 85 (2010) 45–78.
[43] L. Zhang, M. Wang, Theoretical analysis of reverse electrodialysis in nanochannel, J. Eng. Thermophys. 36 (2015) 154–157 (in chinese).
[44] A.J. Kuin, H.N. Stein, Development of a new pore model: Part I. Hydrodynamic and electrical transport phenomena not complicated by surface conductance, J. Colloid Interf. Sci. 108 (1985) 377–388.
[45] S. Levine, G.H. Neale, The prediction of electrokinetic phenomena within multiparticle systems. I. Electrophoresis and electroosmosis, J. Colloid Interf. Sci. 47 (1974) 520–529.
[46] M.W. Kozak, E.J. Davis, Electrokinetic phenomena in fibrous porous media, J. Colloid Interf. Sci. 112 (1986) 403–411.
[47] H. Ohshima, Electroosmotic velocity in fibrous porous media, J. Colloid Interf. Sci. 210 (1999) 397–399.
[48] J.P. Crawshaw, E.S. Boek, Multi-scale imaging and simulation of structure, flow and reactive transport for CO_2 storage and EOR in carbonate reservoirs, Rev. Mineral. Geochem. 77 (2013) 431–458.
[49] S. Torquato, Random heterogeneous media: microstructure and improved bounds on effective properties, Appl. Mech. Rev. 44 (1991) 37.
[50] P.M. Adler, J.F. Thovert, Real porous media: local geometry and macroscopic properties, Appl. Mech. Rev. 51 (1998) 537.
[51] M. Wang, N. Pan, Predictions of effective physical properties of complex multiphase materials, Mater. Sci. Eng.: R: Rep. 63 (2008) 1–30.

[52] D. Hlushkou, A. Seidel-Morgenstern, U. Tallarek, Numerical analysis of electroosmotic flow in dense regular and random arrays of impermeable, nonconducting spheres, Langmuir 21 (2005) 6097–6112.
[53] A. Obliger, M. Jardat, D. Coelho, S. Bekri, B. Rotenberg, Pore network model of electrokinetic transport through charged porous media, Phys. Rev. E 89 (2014) 043013.
[54] M. Wang, J. Wang, N. Pan, S. Chen, Mesoscopic predictions of the effective thermal conductivity for microscale random porous media, Phys. Rev. E 75 (2007) 036702.
[55] S. Chen, G. Doolen, Lattice Boltzmann method for fluid flows, Annu. Rev. Fluid Mech. 30 (1998) 329–364.
[56] G. Karniadakis, A. Beskok, N. Aluru, Microflows and Nanoflows: Fundamentals and Simulation, vol. 29, Springer Science & Business Media, 2006.
[57] M. Wang, X. Lan, Z. Li, Analyses of gas flows in micro- and nanochannels, Int. J. Heat Mass Transf. 51 (2008) 3630–3641.
[58] R.J. Hunter, Foundations of Colloid Science, vol. 1, Clarendon, Oxford, 1989.
[59] A. Negi, S. Anand, A Textbook of Physical Chemistry, Wiley, Eastern, 1985.
[60] R.A. Patel, J. Perko, D. Jacques, G. De Schutter, K. Van Breugel, G. Ye, A versatile pore-scale multicomponent reactive transport approach based on lattice Boltzmann method: application to portlandite dissolution, Phys. Chem. Earth 70–71 (2014) 127–137.
[61] S. Pride, Governing equations for the coupled electromagnetics and acoustics of porous media, Phys. Rev. B 50 (1994) 15678–15696.
[62] A. Yang, C.T. Miller, L.D. Turcoliver, Simulation of correlated and uncorrelated packing of random size spheres, Phys. Rev. E 53 (1996) 1516–1524.
[63] D. Coelho, J.F. Thovert, P.M. Adler, Geometrical and transport properties of random packings of spheres and aspherical particles, Phys. Rev. E 55 (1997) 1959–1978.
[64] S. Bakke, P.-E. Øren, 3-D pore-scale modelling of sandstones and flow simulations in the pore networks, SPE J. 2 (1997) 136–149.
[65] M.S. Talukdar, O. Torsaeter, M.A. Ioannidis, Stochastic reconstruction of particulate media from two-dimensional images, J. Colloid Interf. Sci. 248 (2002) 419–428.
[66] M. Wang, J. He, J. Yu, N. Pan, Lattice Boltzmann modeling of the effective thermal conductivity for fibrous materials, Int. J. Therm. Sci. 46 (2007) 848–855.
[67] J. Wang, M. Wang, Z. Li, Lattice evolution solution for the nonlinear Poisson–Boltzmann equation in confined domains, Commun. Nonlinear Sci. Numer. Simul. 13 (2008) 575–583.
[68] C. Manwart, S. Torquato, R. Hilfer, Stochastic reconstruction of sandstones, Phys. Rev. E 62 (2000) 893–899.
[69] M.S. Talukdar, O. Torsaeter, M.A. Ioannidis, J.J. Howard, Stochastic reconstruction of chalk from 2D images, Transp. Porous Media 48 (2002) 101–123.
[70] J.A. Quiblier, A new three-dimensional modeling technique for studying porous media, J. Colloid Interf. Sci. 98 (1984) 84–102.
[71] P.M. Adler, C.G. Jacquin, J.A. Quiblier, Flow in simulated porous media, Int. J. Multiph. Flow 16 (1990) 691–712.
[72] C.L.Y. Yeong, S. Torquato, Reconstructing random media, Phys. Rev. E 57 (1998) 495–506.
[73] J.F. Thovert, F. Yousefian, P. Spanne, C.G. Jacquin, P.M. Adler, Grain reconstruction of porous media: application to a low-porosity Fontainebleau sandstone, Phys. Rev. E 63 (2001) 061307.
[74] P.M. Adler, Porous Media: Geometry and Transport, Butterworth-Heinemann, Boston, 1992.
[75] C. Aidun, J. Clausen, Lattice-Boltzmann method for complex flows, Annu. Rev. Fluid Mech. 42 (2010) 439–472.
[76] D. Hlushkou, D. Kandhai, U. Tallarek, Coupled lattice-Boltzmann and finite-difference simulation of electroosmosis in microfluidic channels, Int. J. Numer. Methods Fluids 46 (2004) 507–532.
[77] J. Wang, M. Wang, Z. Li, Lattice Poisson-Boltzmann simulations of electro-osmotic flows in microchannels, J. Colloid Interf. Sci. 296 (2006) 729–736.
[78] M. Wang, J. Wang, S. Chen, et al., Electrokinetic pumping effects of charged porous media in microchannels using the lattice Poisson-Boltzmann method, J. Colloid Interf. Sci. 304 (2006) 246–253.
[79] M. Wang, Q. Kang, Modeling electrokinetic flows in microchannels using coupled lattice Boltzmann methods, J. Comput. Phys. 229 (2010) 728–744.
[80] H. Yoshida, T. Kinjo, H. Washizu, Coupled lattice Boltzmann method for simulating electrokinetic flows: a localized scheme for the Nernst–Plank model, Commun. Nonlinear Sci. Numer. Simul. 19 (2014) 3570–3590.
[81] L. Zhang, M. Wang, Modeling of electrokinetic reactive transport in micropore using a coupled lattice Boltzmann method, J. Geophys. Res.: Solid Earth 120 (2015) 2877–2890.
[82] A.J.C. Ladd, Numerical simulations of particulate suspensions via a discretized Boltzmann equation. Part 1. Theoretical foundation, J. Fluid Mech. 271 (1994) 285.
[83] J.T.G. Overbeek, Colloid science, Irreversible Systems, vol. 1, Elsevier Publishing Company, Amsterdam, 1952.
[84] P.C. Carman, Flow of Gases through Porous Media, Academic Press, 1956.
[85] D.L. Johnson, J. Koplik, R. Dashen, Theory of dynamic permeability and tortuosity in fluid-saturated porous media, J. Fluid Mech. 176 (1987) 379–402.
[86] N. Epstein, On tortuosity and the tortuosity factor in flow and diffusion through porous media, Chem. Eng. Sci. 44 (1989) 777–779.
[87] E.B. Cummings, S.K. Griffiths, R.H. Nilson, P.H. Paul, Conditions for similitude between the fluid velocity and electric field in electroosmotic flow, Anal. Chem. 72 (2000) 2526–2532.
[88] R.F. Probstein, Physicochemical Hydrodynamics: An Introduction, John Wiley & Sons, 2005.